JAERI-M
89-209

# STUDY OF MARFE PHENOMENA ON JT-60

December 1989

Takeo NISHITANI and Shin-ichi ISHIDA

日 本 原 子 力 研 究 所
Japan Atomic Energy Research Institute

JAERI-Mレポートは，日本原子力研究所が不定期に公刊している研究報告書です。
入手の問合わせは，日本原子力研究所技術情報部情報資料課（〒319-11茨城県那珂郡東海村）あて，お申しこしください。なお，このほかに財団法人原子力弘済会資料センター（〒319-11 茨城県那珂郡東海村日本原子力研究所内）で複写による実費頒布をおこなっております。

JAERI-M reports are issued irregularly.
Inquiries about availability of the reports should be addressed to Information Division Department of Technical Information, Japan Atomic Energy Research Institute, Tokai-mura, Naka-gun, Ibaraki-ken 319-11, Japan.



編集兼発行　日本原子力研究所
印　　刷　いばらき印刷㈱

JAERI-M 89-209

# Study of Marfe Phenomena on JT-60

Takeo NISHITANI and Shin-ichi ISHIDA

Department of Large Tokamak Research
Naka Fusion Research Establishment
Japan Atomic Energy Research Institute
Naka-machi, Naka-gun, Ibaraki-ken

(Received November 15, 1989)

The marfe (Multifaceted Asymmetric Radiation From the Edge) is a poloidally asymmetric radiation band localized near the inside midplane and is a common phenomenon among middle and large size tokamaks like Alcator-C, ASDEX, TFTR and JET. In JT-60 marfe has been observed frequently in high-Ip and high density limited discharges with neutral beam heating. It can be explained as a radiative thermal instability caused by light impurities in a peripheral plasma. Though the marfe onset close to the density limit reduces the line averaged electron density, it does not affect the central electron temperature and the energy confinement. The marfe onset at relatively low Ip improves energy confinement time up to several % accompanied with the increase of electron density.

Keywords: Marfe, Radiative Thermal Instability, Peripheral Plasma Radiation Loss, JT-60, Bolometer, Light Impurity

JAERI－M 89－209

# JT－60におけるmarfe現象の研究

日本原子力研究所那珂研究所臨界プラズマ研究部
西谷　健夫・石田　真一

（1989年11月15日受理）

marfe（Multifaceted Asymmetric Radiation From the Edge）は，トーラス内側のプラズマ表面近傍の帯状の領域に局在して放射損失が強まる現象であり，不純物の放射冷却に起因する熱的不安定性である。帯の幅は，ポロイダル角にして15～30°でトロイダル方向にはほぼ一様であり，強BTつまり内側の赤道面付近に発生する。この現象は，Alcator－C，ASDEX，DIII－D，JET，TFTRなどほとんどの中，大型トカマク装置で共通に見られる現象である。JT－60では，TiC被覆モリブデン壁のときは2，3の例以外観測されなかったが，グラファイトタイルに交換してからは高プラズマ電流（2 MA以上）のリミター配位において高パワー（10～20 MW）のNBI加熱中に頻繁に発生するようになった。このmarfeは密度限界近傍で発生し，電子密度の低下させるもの中心電子温度には影響を与えず，著しいプラズマの閉じ込め劣化をもたらさないことがわかった。また，最近（1988～1989年）比較的低プラズマ電流（1～1.5 MA）で観測されたmarfeは電子密度の上昇を伴い，プラズマの閉じ込めを数%程度改善することがわかった。

那珂研究所：〒311－01　茨城県那珂郡那珂町大字向山801－1

# Contents



# 目　　次

## 1. INTRODUCTION

The edge plasma has been studied from the point of view of the plasma surface interactions such as sputtering or sublimation of the first wall and the impurity control such as divertor. Recently it has been revealed that the improvement of confinement such as H-mode [1,2] and IOC [3,4] are related with the edge plasma conditions. So the importance of edge plasma physics has been recognized as an improving effect on core plasma confinement.

A marfe, multifaceted asymmetric radiation from the edge, is one of the edge plasma phenomena regarded as a radiated thermal instability. As shown in Fig.1 a marfe is a toroidally symmetric and poloidally asymmetric radiating belt localized on the inside wall near the midplane where is the high field edge of the plasma. The width of the marfe is 15-30 ° of poloidal angle. The phenomena was reported at ASDEX [5,6] and D-III [7] previously, Lipschltz [8] investigated it precisely in ohmically heated Alcator-C plasma and named it marfe. Now the marfe is a common phenomena among the middle and large size tokamak such as JET [9-11], TFTR [12-14] and FT [15]. Though almost plasmas occurring marfe are ohmically heated limiter discharged in those tokamaks, the marfe in diverted discharges has been observed only on ASDEX [5]. The marfe in the plasma with intense neutral beam (NB) heating has not reported.

On JT-60 the marfe had not been observed in the discharges with TiC coated molybdenum first wall except only several ones in the high density ohmically heated discharges. After replacement of TiC coated molybdenum first wall by graphite tills, marfe has been observed frequently in high Ip, 2.5-3.2MA, limited discharges with high power NB heating of 10-20MW. The marfe occurs close to the density limit and reduces the $\overline{n_e}$, but it does not affect the central electron temperature and the energy confinement. Recently marfe has been observed in the relatively low Ip and $\overline{n_e}$ which results in improvement of energy confinement time up to several % accompanied with the increase of electron density.

Section 2 shows the theory of the marfe. Section 3 describes the diagnostics concerned with marfe observation. The characteristics of the marfe observed on JT-60 are shown in Section 4. Section 5 discusses the detached plasma transition and application of marfe. Section 6 is the summary and conclusion.

## 2. THEORY OF MARFE

The marfe is considered to be the result of a radiative thermal instability due to light impurity in peripheral plasma. The radiation loss of an impurity is given by

$$P_{rad} = n_e n_Z L_Z(T_e) \tag{1}$$

where $n_e$ is the electron density, $n_Z$ is the impurity density, and $L_Z(T_e)$ is the radiation cooling rate. Because the $L_Z$ of light impurity such as carbon and oxygen has a negative vallue of $dL_Z/dT$, the temperature becomes lower and lower once it decreases. Simple model of the marfe is reported by Lipschultz [8] and Baker [7]. More precise model based on Stringer's model [19] is as follows.

The energy balance equation is given by

$$3\frac{\partial(nT)}{\partial t} = \frac{\partial}{\partial s}\left\{K_{\|}\frac{\partial T}{\partial s} - 5nTv_{\|}\right\} + \frac{1}{r}\frac{\partial}{\partial r}\left\{rK_{\perp}\frac{\partial T}{\partial r}\right\} - \sum nn_Z L_Z(T) \tag{2}$$

where $n=n_e=n_i$ and $T=T_e=T_i$, s is a distance along a field line, $K_{\perp}$ and $K_{\|}$ perpendicular and parallel conductivities respectively. The derivatives along field lines can be converted to derivatives in poloidal angle as

$$\frac{\partial}{\partial s} = \frac{\Theta}{r}\frac{\partial}{\partial \theta} \tag{3}$$

where $\Theta$ is a pitch angle defining by $B_P/B_T$. Since marfes are observed to be toroidal symmetric, the temperature and density perturbation are assumed to be functions only of poloidal angle and minor radius as follows;

$$\tilde{T}(r,\theta,t) = \tilde{T}(r)e^{\gamma t}\cos m\theta \tag{4}$$

To obtain a dispersion equation for $\gamma$, Eq. (1) is linearized and combined with the continuity equation and the parallel component of the fluid equation of motion. By assuming the fractional density perturbation of the impurity to be equal to that of the electrons and

$$\gamma\left[\gamma^2+\frac{5}{3}\frac{2T}{M}k_{\|}^2\right] = \frac{1}{3n}\left[K_{\|}k_{\|}^2+\frac{K_{\perp}}{\Delta^2}+nn_Z\frac{dL_Z}{dT}\right]\left[\gamma^2+\frac{2T}{M}k_{\|}^2\right]+\frac{4}{3}\frac{n_Z L_Z}{M}k_{\|}^2 \tag{5}$$

is obtained, where $k_{\parallel}^2 = m^2\Theta^2/r^2$. In deriving Eq. (5), the perpendicular heat conduction term in Eq. (1) is replaced by $-K_{\perp}\tilde{T}/\Delta^2$ where $\Delta$ is the radial half width of the perturbed layer. The condition for instability ($\gamma > 0$) is

$$K_{\parallel}k_{\parallel}^2 + \frac{K_{\perp}}{\Delta^2} - \frac{2nn_Z L_Z}{T} + nn_Z\frac{dL_Z}{dT} < 0 \qquad (6)$$

The first and second terms in Eq. (6) are the parallel and perpendicular heat conduction respectively, the former is usually more important than the latter. The third and fourth terms in Eq. (6) express the change in radiation due to density and temperature variations respectively. if the perpendicular heat conduction term is neglected and m is assumed to be unity, the edge density condition for marfe onset is given from Eq. (6) by

$$n_e > \frac{K_{\parallel}k_{\parallel}^2}{n_Z\left\{\frac{2L_Z}{T} - \frac{dL_Z}{dT}\right\}} = \frac{K_{\parallel}}{R^2q^2n_Z\left\{\frac{2L_Z}{T} - \frac{dL_Z}{dT}\right\}}. \qquad (7)$$

Generally impurity ions in the edge plasma are not coronal equilibrium, however, the critical electron density for marfe onset can be estimated by using non-coronal model of $L_Z$ such as Carolan's [20].

## 3. DIAGNOSTICS CONCERNED WITH MARFE

The sightlines of the diagnostics concerned with the marfe observation are shown in Fig.2. The behavior of the marfe can be observed by a bolometer array most effectively. On JT-60 the bolometer array consisting of 15 channel metal bolometers [21] installed in the bottom diagnostics port outside the vacuum vessel measures radiated powers from the plasma more than a half of the poloidal cross-section. Recently another array consisting of 16 channel bolometers was installed in the top diagnostics port outside the vacuum vessel. Four channel of Hα monitors using photodiode with Hα bandpassing filter [22], two channel of VUV spectrometers [23] measure Hα emissions and impurity lines, respectively in the same toroidal section as the bolometer array. Note that the Hα monitor signals involve the CII line of 657.6 nm because the Hα banpassing filters have 10 nm of the FWHM centered at 656.3 nm. Additional thermistor bolometers and Hα monitors are installed at three

is obtained, where $k_{\parallel}^2 = m^2\Theta^2/r^2$. In deriving Eq. (5), the perpendicular heat conduction term in Eq. (1) is replaced by $-K_{\perp}\tilde{T}/\Delta^2$ where $\Delta$ is the radial half width of the perturbed layer. The condition for instability ($\gamma > 0$) is

$$K_{\parallel}k_{\parallel}^2 + \frac{K_{\perp}}{\Delta^2} - \frac{2nn_Z L_Z}{T} + nn_Z\frac{dL_Z}{dT} < 0 \qquad (6)$$

The first and second terms in Eq. (6) are the parallel and perpendicular heat conduction respectively, the former is usually more important than the latter. The third and fourth terms in Eq. (6) express the change in radiation due to density and temperature variations respectively. if the perpendicular heat conduction term is neglected and m is assumed to be unity, the edge density condition for marfe onset is given from Eq. (6) by

$$n_e > \frac{K_{\parallel}k_{\parallel}^2}{n_Z\left\{\frac{2L_Z}{T} - \frac{dL_Z}{dT}\right\}} = \frac{K_{\parallel}}{R^2q^2n_Z\left\{\frac{2L_Z}{T} - \frac{dL_Z}{dT}\right\}}. \qquad (7)$$

Generally impurity ions in the edge plasma are not coronal equilibrium, however, the critical electron density for marfe onset can be estimated by using non-coronal model of $L_Z$ such as Carolan's [20].

## 3. DIAGNOSTICS CONCERNED WITH MARFE

The sightlines of the diagnostics concerned with the marfe observation are shown in Fig.2. The behavior of the marfe can be observed by a bolometer array most effectively. On JT-60 the bolometer array consisting of 15 channel metal bolometers [21] installed in the bottom diagnostics port outside the vacuum vessel measures radiated powers from the plasma more than a half of the poloidal cross-section. Recently another array consisting of 16 channel bolometers was installed in the top diagnostics port outside the vacuum vessel. Four channel of Hα monitors using photodiode with Hα bandpassing filter [22], two channel of VUV spectrometers [23] measure Hα emissions and impurity lines, respectively in the same toroidal section as the bolometer array. Note that the Hα monitor signals involve the CII line of 657.6 nm because the Hα banpassing filters have 10 nm of the FWHM centered at 656.3 nm. Additional thermistor bolometers and Hα monitors are installed at three

vertical diagnostics ports at R=2.53 m, 3.04 m, and 3.55 m. A visible TV is a helpful to see the marfe behavior directly. On JT-60 a visible TV camera is installed in the top diagnostics port outside the vacuum vessel and views the inside wall vertically against the magnetic axis. The electron density of the main plasma is measured with FIR interferometers with three vertical chords ( R=2.53 m, 3.04 m, and 3.55 m ) and 2 mm wave interferometer at R=2.2 m [24] where is the marfe region.

## 4. PHENOMENOLOGY OF MARFE ON JT-60

### 4.1 Outline of Marfe Phenomena

The marfe had not been observed in the discharges with TiC coated molybdenum first wall except several ohmically heated discharges with new configuration where the plasma had a separatrix line and touched to the inboard limiter by exciting the divertor coil weakly. This experiments were carried out from January to March 1987 just before the replacement of the first wall to the graphite tiles. Figure 3 shows the typical configuration of the discharges. The typical waveforms of the marfe in ohmically heated plasma are shown in Fig.4. The radiated power increased rapidly at 5.7 sec. The gas puffing kept constant from 1 sec to 7 sec. The line-integrated electron density which was increasing until 5.7 sec saturated from 5.7 sec to 6.2 sec and began to increase steeply. The enhanced radiation from 5.7 sec to 8.5 sec is the marfe, which is indicated clearly by the time evolution of the chord-integrated radiation losses shown in Fig. 5. The radiation is enhanced around channel 11 which views inside wall 28.5° above the midplane. There is not enhancement of the intensity of the bolometer signal with vertical viewing chord passing the plasma center and the increase of Hα intensity is most remarkable among the three vertical Hα monitors. These facts indicate that the enhanced radiation is localized near the inside wall. The light impurity spectrometers were not operated routinely in the period, so we do not have the information of the light impurity behavior in the marfe.

After replacement of TiC coated molybdenum first wall to graphite tills, marfe has been observed frequently in high Ip, 2.5-3.2MA, limited discharges with high power NB heating of 10-20MW. Figure 6 shows the typical waveformes of the parameters of the discharge with the marfe. The marfe occurs at 6.6 sec. Then the intensities of the bolometer and the Hα monitor viewing the inner wall on the midplane increase steeply. Remarkable changes

vertical diagnostics ports at R=2.53 m, 3.04 m, and 3.55 m. A visible TV is a helpful to see the marfe behavior directly. On JT-60 a visible TV camera is installed in the top diagnostics port outside the vacuum vessel and views the inside wall vertically against the magnetic axis. The electron density of the main plasma is measured with FIR interferometers with three vertical chords ( R=2.53 m, 3.04 m, and 3.55 m ) and 2 mm wave interferometer at R=2.2 m [24] where is the marfe region.

## 4. PHENOMENOLOGY OF MARFE ON JT-60

### 4.1 Outline of Marfe Phenomena

The marfe had not been observed in the discharges with TiC coated molybdenum first wall except several ohmically heated discharges with new configuration where the plasma had a separatrix line and touched to the inboard limiter by exciting the divertor coil weakly. This experiments were carried out from January to March 1987 just before the replacement of the first wall to the graphite tiles. Figure 3 shows the typical configuration of the discharges. The typical waveforms of the marfe in ohmically heated plasma are shown in Fig.4. The radiated power increased rapidly at 5.7 sec. The gas puffing kept constant from 1 sec to 7 sec. The line-integrated electron density which was increasing until 5.7 sec saturated from 5.7 sec to 6.2 sec and began to increase steeply. The enhanced radiation from 5.7 sec to 8.5 sec is the marfe, which is indicated clearly by the time evolution of the chord-integrated radiation losses shown in Fig. 5. The radiation is enhanced around channel 11 which views inside wall 28.5° above the midplane. There is not enhancement of the intensity of the bolometer signal with vertical viewing chord passing the plasma center and the increase of Hα intensity is most remarkable among the three vertical Hα monitors. These facts indicate that the enhanced radiation is localized near the inside wall. The light impurity spectrometers were not operated routinely in the period, so we do not have the information of the light impurity behavior in the marfe.

After replacement of TiC coated molybdenum first wall to graphite tills, marfe has been observed frequently in high Ip, 2.5-3.2MA, limited discharges with high power NB heating of 10-20MW. Figure 6 shows the typical waveformes of the parameters of the discharge with the marfe. The marfe occurs at 6.6 sec. Then the intensities of the bolometer and the Hα monitor viewing the inner wall on the midplane increase steeply. Remarkable changes

are not observed in the one turn voltage, SX intensities and sawtooth activity. Though the gas puffing is continuous, the increase of the electron density saturates at the marfe onset. It is suggesting that the marfe degrades the fueling efficiency of the gas puffing. Figure 7 shows the time evolution of the chord-integrated radiation losses measured with the bolometer array. The intensity of the ch. 1 bolometer is increasing from 5.5 to 6.6 sec with the increase of the electron density. The intensities of the ch.5-ch.10 increases rapidly at the same time as the decrease of the ch. 1 intensity. The enhanced radiation is kept for about two second until the end of NB injection.

### 4.2 Onset Position and Poloidal Motion

If the marfe is assumed to be localized on the inner wall, the poloidal spread of the marfe can be estimated from the chord-integrated radiation profile such as Fig.7. The poloidal extent of the marfe is shown in Fig.8. The center of the marfe is about 10° above the midplane and the FWHM of the radiative band is 15° of poloidal angle. The visible TV camera observes the bright emission of the toroidal band corresponding to the radiative band as shown in Fig.9. The marfe occurs on the midplane ($\theta \sim 180°$) in ASDEX, FT and D-III, and above the midplane ($\theta \sim 120°$) in Alcator-C, and below the midplane ($\theta \sim 235°$) in TFTR and JET. Though the radial extent of the marfe has not been measured directly on JT-60, it is said generally to be about 10% of the plasma minor radius [25]. The radiation power density in the marfe is estimated to be more than $30MW/m^3$ from Fig.8 if the radial extent of the marfe assumed to be 0.1 m.

The marfe sometimes moves upward in JT-60. The drift motion appears often while the plasma current is ramping down and/or NB power is reduced fully or partially. Figures 10 and 11 show the two dimensional plot and contour plot of the time evolution of the chord-integrated radiation losses of the marfe onset when the NB power reduces 50% and the configuration is changed from the outer X-point divertor to the limiter. The marfe drifts from 174° to 150° of the poloidal angle with the angular velocity of about 30°/sec. which is much slower than that of other tokamaks such as Alcator-C. In TFTR the direction of the drift motion is correspond to the $\mathbf{B}\times\nabla\mathbf{B}$, which is confirmed by the reverse of the toroidal field. Whereas the direction of the drift motion is upward independent of the $B_T$ direction in JT-60.

### 4.3 Impurity Behavior

The time evolutions of light impurity brightness in the marfe measured by the normal incidence spectrometer [23] are shown in Fig. 12. Major lines of low-ionized light impurities are saturated before the marfe onset, so that relatively week lines are employed here for the interpretation of impurity behvior. In this discharge, the marfe occurred at 7 sec triggered by the 25% turnoff of the NB injection. Then the brightnesses of CII, CIII and OII lines increases steeply to be saturated. whereas, the brightnesses of CIV and Lyβ lines decreases to be unsaturated level from saturation level. It is suggested that the low-ionized carbon and oxygen are major radiation source in the marfe. In JET, enhancement factors of low-ionized carbon and oxygen by marfe onset was investigated quantitatively [25] as shown in Fig. 13. The enhancement factors of CIII, OII and OIII are largest. Figure 14 shows diagnostics wave forms of the marfe in relatively low density and plasma current plasma with NB heating on JT-60 including the time evolutions of CVI and OVIII brightnesses measured with VUV spectrometer viewing plasma center. The brightness of CVI increases according to the increase of electron density in marfe period, however, that of OVIII decreased. It can be estimated that the concentration of oxygen reduces with the marfe onset.

### 4.4 Density Behavior

The increases of chord-integrated electron densities along the three vertical chords at R=2.53, 3.04 and 3.55 m are saturated with same manner at the marfe onset in spite of continuous gas puffing as shown in Fig. 15 (a). In the discharge shown in Fig. 15 (b), the chord-integrated density decreases ones at the marfe onset and keeps rising within the marfe period resulting in a major disruption at density limit, which is a only rare case. The density degradation by the marfe is helpful to avoid the density limit disruption in many cases on JT-60. Similar density degradation has been observed in center and outer side of the TFTR plasma [18). However, the density in the vicinity of the marfe increases. In JT-60, the density behavior in the vicinity of the marfe could not investigated because the 2 mm interferometer at R=2.2 m could not available due to the fringe counting error by large density gradient at the peripheral region. In relatively low density and plasma current plasmas with NB heating, the density increases in the marfe period as shown in Fig, 14. Similar density increase have been observed in Alcator-C [12] and ASDEX [11].

The mechanisms of these two types of density behaviors are unknown at present.

### 4.5 Onset Condition

The Hugill diagram of the plasma at the marfe onset and the plasma disrupted by density limit is shown in Fig. 16. It is indicated that the marfe is observed in the vicinity of the density limit. Figures 17 (a) and 17 (b) show the time trajectories in the Hugill diagram for the plasmas with marfe onset at constant $I_P$ phase and decreasing $I_P$ phase, respectively. In the constant $I_P$, the marfe occurs on the density limit, whereas the marfe occurs in the density region higher than the density limit in decreasing $I_P$ where the poloidal drift motion of the marfe has been observed frequently.

The threshold electron density for the marfe onset is plotted against the plasma current normalized by the poloidal cross-section of the plasma in Fig. 18. Defining $\rho$ to be $\overline{n_e}/(I_P/\pi a^2)$, $\rho = 0.55 \pm 0.05$ for ohmically heated plasma and $\rho = 0.90 \pm 0.15$ for NB heated plasma on JT-60. The scatter of the $\rho$ is seemed to be due to the NB power and condition of plasma current (rising, flattop, and falling). The comparison of the $\rho$ with that of the other tokamaks is summarized in Table 1 as Lipschultz showed in Ref. [25]. The $\rho$ is about 0.5 and 0.9 for ohmic and NB heated plasma, respectively in other tokamaks, which is consistent with the results of JT-60.

The NB power dependence of the threshold density for the marfe onset is investigated in several discharges where the NB powers are different but the other conditions are almost same. The threshold density increases with the increase in the NB power as shown in Fig. 19. In other words, the marfe is suppressed by the NB injection. The empirical scaling of the marfe onset taking account of the NB power is derived from Fig. 19 as

$$\overline{n_e} = (\rho_{OH} I_P + \rho_{NB} P_{NB})/\pi a^2 \qquad (8)$$

where

$$\rho_{OH} = 0.55 \pm 0.05 \ \ (10^{20}/\mathrm{MAm})$$

$$\rho_{NB} = 0.07 \pm 0.01 \ \ (10^{20}/\mathrm{MWm}).$$

The validity of the scaling would be confirm for the other tokamaks.

Table 1 Threshold Density of Marfe Onset Normalized by the Poloidal Cross-section on Various Tokamaks

| Machine | R (m) | a (m) | $B_T$ (T) | $\rho = \overline{n_e}/(I_P/\pi a^2)$ | Comments |
|---|---|---|---|---|---|
| JT-60 | 3.04 | 0.9 | 4 | $0.55 \pm 0.05$ | OH |
| | 3.04 | 0.9 | 4.75 | $0.9 \pm 0.15$ | NBI |
| Alcator-C | 0.64 | 0.165 | 6-10 | $0.5 \pm 0.05$ | OH |
| ASDEX | 1.65 | 0.4 | 2.2 | $0.7 \pm 0.05$ | OH, diverted |
| | 1.65 | 0.4 | 2.2 | $0.5 \pm 0.05$ | NBI |
| D-III | 1.4 | 0.4 | 2 | 0.45 | OH |
| JET | 2.96 | 1.25 | 2.5--3.4 | 0.55 - 0.3 | OH |
| TFTR | 2.5 | 0.82 | 4 | $0.4 \pm 0.05$ | OH |
| FT | 0.83 | 0.2 | 6-8 | $0.75 \pm 0.05$ | OH, $I_P$ down |

## 4.6 Global Power Balance and Energy Confinement

In general, the total radiated power is derived from the volume integration of the radiation profile, $P_{rad}(r)$, which is provided by the Abel inversion of the bolometer array signals, where the radiation profile assumed to be axisymmetric. The method, however, is not valid for the plasma with poloidally asymmetric radiation profile like marfe. Therefor symmetric component and marfe component of the total radiated power are calculated individually by separating the bolometer signals to each component as shown in Fig. 8, where symmetric component of the marfe viewing channel is estimated from that of the other channels by interpolation. The time evolutions of the symmetric and marfe components of the total radiated power for the plasma as for Fig. 4 are shown in Fig. 20. In this discharge, the power radiated from the marfe is up to 50% of the total radiated power, however, it is 20-50% useally in other discharges.

The fractional radiated power to the absorbed power in the NB heated limiter discharges with graphite first wall as a function of $\overline{n_e}$ is shown in Fig. 21. The radiated power is 25% of the absorbed power in the range of the $\overline{n_e}$ from $1\times10^{19}$ to $6\times10^{19}$ $m^{-3}$ almost independent of $\overline{n_e}$. With the increase in the $\overline{n_e}$ larger than $6\times10^{19}m^{-3}$, The fractional radiated power increases steeply to be up to 70%. In these plasma radiated power from the peripheral region contributes the increase of the total radiated power. Near the density limit,

marfe appears on the inside wall. The radiated power from the plasma with marfe reaches up to 90% of the absorbed power.

Figure 22 shows the time evolutions of the stored energy measured by the diamagnetic loop, the electron temperature measured from the ECE emission, and other parameters as for Fig. 4. Both stored energy and electron temperatures do not changes by the marfe onset at 6.6 sec in spite of the intense radiation loss. In the marfe of relatively low density and $I_P$, the stored energy increases accompany with the increase of the electron density as shown in Fig. 23. Reducing the increase of stored energy due to decreasing NB shinethrough with the increase of density, the energy confinement time is improved about 5%. The effect of marfe on the energy confinement has not been refered in papers for other tokamaks. But it was presented from Alcator-C in Ref. [8] that the influx of molybdenum was suppressed by the marfe. One possibility of the improvement by the marfe is that the marfe reduces the temperature of the edge plasma and suppresses the particle recycling and impurity influx from the first wall.

## 5. DISCUSSION

The local emissivity is typically 30 MW/m$^3$ in the marfe. Possible energy loss channels contributing to this large emissivity value are (a) atomic and molecular hydrogen radiation, charge-exchange neutral emission, and low-Z impurity radiation.

Atomic and molecular hydrogen radiation could not estimated because the H$\alpha$ monitors saturated in the marfe period and spectrometers were not calibrated. Some CX neutral particle analyzers are installed on the outside of the torus. they could not measure the charge-exchange neutral emission from the marfe because the neutral particles from the marfe would re-ionize by passing the main plasma. Lipschultz [8] indicated that these two processes were not significant energy loss channels from the marfe region.

The remaining process which could account for the large value of local radiated power in the marfe is line emission from the light impurities. So a preliminary estimation of the light impurity concentration was parformed by using Eq. (1) as

$$\frac{n_Z}{n_e} = \frac{P_{rad}}{n_e^2 L_Z} . \qquad (9)$$

marfe appears on the inside wall. The radiated power from the plasma with marfe reaches up to 90% of the absorbed power.

Figure 22 shows the time evolutions of the stored energy measured by the diamagnetic loop, the electron temperature measured from the ECE emission, and other parameters as for Fig. 4. Both stored energy and electron temperatures do not changes by the marfe onset at 6.6 sec in spite of the intense radiation loss. In the marfe of relatively low density and $I_P$, the stored energy increases accompany with the increase of the electron density as shown in Fig. 23. Reducing the increase of stored energy due to decreasing NB shinethrough with the increase of density, the energy confinement time is improved about 5%. The effect of marfe on the energy confinement has not been refered in papers for other tokamaks. But it was presented from Alcator-C in Ref. [8] that the influx of molybdenum was suppressed by the marfe. One possibility of the improvement by the marfe is that the marfe reduces the temperature of the edge plasma and suppresses the particle recycling and impurity influx from the first wall.

## 5. DISCUSSION

The local emissivity is typically 30 MW/m$^3$ in the marfe. Possible energy loss channels contributing to this large emissivity value are (a) atomic and molecular hydrogen radiation, charge-exchange neutral emission, and low-Z impurity radiation.

Atomic and molecular hydrogen radiation could not estimated because the H$\alpha$ monitors saturated in the marfe period and spectrometers were not calibrated. Some CX neutral particle analyzers are installed on the outside of the torus. they could not measure the charge-exchange neutral emission from the marfe because the neutral particles from the marfe would re-ionize by passing the main plasma. Lipschultz [8] indicated that these two processes were not significant energy loss channels from the marfe region.

The remaining process which could account for the large value of local radiated power in the marfe is line emission from the light impurities. So a preliminary estimation of the light impurity concentration was parformed by using Eq. (1) as

$$\frac{n_Z}{n_e} = \frac{P_{rad}}{n_e^2 L_Z} . \qquad (9)$$

Here Prad is 30 MW/$m^3$, $n_e$ is assumed to be $5 \times 10^{19}$ $m^{-3}$ and $T_e$ is assumed to be 10 eV in the marfe region. If the impurity is assumed to be carbon and $n_e\tau$ is assumed to be $10^{17}$ $m^{-3}$, $L_Z$ is $1 \times 10^{-31}$ $Wm^3$ and averaged charge state is about three from non-coronal model [20]. The $n_Z/n_e$ of about 0.1 is estimated. So the local $Z_{eff}$ value of about 1.5 are required to explain the observed radiation emissivity.

In some tokamaks [14-16], the marfe expands to be poloidally symmetric radiative shell. The temperature of the region is so low that the radius of the hot plasma becomes effectively smaller than that of the limiter. Therefor the plasma is called a detached plasma. The detached plasma is characterized the strong radiation emmisivity at the plasma boundary formed approximately uniform in poloidal and toroidal angles with the total amount of radiation equal to the input power, where energy and particle confinements are improved. In JT-60, the transition of the detached plasma from marfe has not been observed yet.

The marfe and detached plasma would be favorable operational regime to provide the remote radiative cooling for tokamaks without divertor.

## 6. CONCLUSION

The marfe is a poloidally asymmetric radiation band localized near the inside midplane and is a common phenomenon among middle and large size tokamaks. There are many reports on the marfe in ohmic plasmas but few on in the NB heated plasmas The marfe phenomena has been investigated in NB heated plasma on JT-60. The marfe can be explained as a radiative thermal instability in a peripheral plasma. The marfe is caused by light impurities in low charge states such as carbon and oxygen. The threshold electron density for the marfe onset normalized by averaged current density, $\rho = \overline{n_e}/(I_P/\pi a^2)$, is $0.55 \pm 0.05$ for ohmically heated plasma and $0.90 \pm 0.15$ for NB heated plasma on JT-60, which is consistent with the results of other tokamaks. Though the marfe onset close to the density limit reduces the line averaged electron density, it does not affect the central electron temperature and the energy confinement. The marfe onset at relatively low Ip improves energy confinement time up to several % accompanied with the increase of electron density.

Here Prad is 30 MW/$m^3$, $n_e$ is assumed to be $5 \times 10^{19}$ $m^{-3}$ and $T_e$ is assumed to be 10 eV in the marfe region. If the impurity is assumed to be carbon and $n_e\tau$ is assumed to be $10^{17}$ $m^{-3}$, $L_Z$ is $1 \times 10^{-31}$ $Wm^3$ and averaged charge state is about three from non-coronal model [20]. The $n_Z/n_e$ of about 0.1 is estimated. So the local $Z_{eff}$ value of about 1.5 are required to explain the observed radiation emissivity.

In some tokamaks [14-16], the marfe expands to be poloidally symmetric radiative shell. The temperature of the region is so low that the radius of the hot plasma becomes effectively smaller than that of the limiter. Therefor the plasma is called a detached plasma. The detached plasma is characterized the strong radiation emmisivity at the plasma boundary formed approximately uniform in poloidal and toroidal angles with the total amount of radiation equal to the input power, where energy and particle confinements are improved. In JT-60, the transition of the detached plasma from marfe has not been observed yet.

The marfe and detached plasma would be favorable operational regime to provide the remote radiative cooling for tokamaks without divertor.

## 6. CONCLUSION

The marfe is a poloidally asymmetric radiation band localized near the inside midplane and is a common phenomenon among middle and large size tokamaks. There are many reports on the marfe in ohmic plasmas but few on in the NB heated plasmas The marfe phenomena has been investigated in NB heated plasma on JT-60. The marfe can be explained as a radiative thermal instability in a peripheral plasma. The marfe is caused by light impurities in low charge states such as carbon and oxygen. The threshold electron density for the marfe onset normalized by averaged current density, $\rho = \overline{n_e}/(I_P/\pi a^2)$, is $0.55 \pm 0.05$ for ohmically heated plasma and $0.90 \pm 0.15$ for NB heated plasma on JT-60, which is consistent with the results of other tokamaks. Though the marfe onset close to the density limit reduces the line averaged electron density, it does not affect the central electron temperature and the energy confinement. The marfe onset at relatively low Ip improves energy confinement time up to several % accompanied with the increase of electron density.

## ACKNOWLEDGEMENTS

The author would like to thank Drs N. Hosogane, K. Nagashima, and H. Takeuchi for their fruitful discussions. The continuing supports of Drs. M. Yoshikawa, S. Tamura, and A. Funahashi are gratefully acknowledged.

## REFERENCES


[1] F. Wagner, G. Becker, K. Behringer, D. Campbell and A. Eberhagen, Phys. Rev. Lett. **49** (1982) 1408.

[2] N. Ohyabu, G. Jahns, R. Sambough and E. Strait, Phys. Rev. Lett. **58** (1982) 120.

[3] F. Söldner, E. Müller, F. Wagner, et al., Phys. Rev. Lett. **61** (1988) 1105.

[4] G. Fussmann, O. Gruber, H. Ntedermeyer, et al., in Plasma Physics and Controlled Nuclear Fusion Research 1988 (Proc. 12 the Int. Conf. Nice 1988) IAEA-CN-50/A-3-1.

[5] H. Niedermeyer, K. Behrimger, K. Bernhardi, A. Eberhagen, G. Fusmann, et al., Max-Planck-Institute für Plasmaphysik, Garching Report IPP-III/90 (1983).

[6] H. Niedermeyer, R. Bartiromo, G. Becker, H.S. Bosch, H. Brocken et al., in Proc. 12th European Conf. on Controlled Fusion and Plasma Physics, Budapest, Hungary, 1985, contributed papers, Part I, P. 159.

[7] D.R. Baker, R.T. Snider and M. Nagami, Nucl. Fusion **22** (1982) 807.

[8] B. Lipschults, B. LaBonbard, E.S. Markar, M.M. Pichkrell, J.L. Terry, R. Watterson and S.M. Wolfe, Nucl. Fusion **24** (1984) 977.

[9] J. Wesson, C. Gowers, W. Han, F. Mast, F. Nave, M. Turner and M. Watkins, in Proc. 12th European Conf. on Controlled Fusion and Plasma Physics, Budapest, Hungary, 1985, contributed papers, Part I, P. 147.

[10] J. O'Rouurke, D. Campbell, B. Denne, A. Gondhalker, N. Gottardi, H. Krause, G. Magyar, M. Malacarne, F. Mast, P. Morgan, M.F. Nave, F.C. Schüller, M. Stamp and D. Summers, ibid, P. 155.

[11] P.G. Carolan, M.J. Forrest, N.C. Hawkwes and N.J. Peacock, ibid, P. 263.

[12] F.P. Boody, C.E. Bush, S.S. Medley, H.K. Park and J.F. Schivell, J. Nucl. Mater. **145-147** (1987) 196.

[13] J. Schivell and C.E. Bush, Rev. Sci. Instrum. **57** (1986) 2081.

[14] J. Schivell, Rev. Sci. Instrum. **58** (1987) 12.

[15] F. Alladio, R. Bartiromo, B. Casali, P. Buratti, F. De Marco, , M. De Pretis, R. Giannellla, M. Grolli, L. Pieloni, A Tanga, A. Tuccillo and O. Tudiso, Phys. Lett. **90A** (1982) 405.

[16] J.D. Strachan et al., in Proc. 12th European Conf. on Controlled Fusion and Plasma Physics, Budapest, Hungary, 1985, contributed papers, Part I, P. 339.

[17] J.D. Strachan, F.P. Boody, C.E. Bush, S.A. Cohen, B. Grek, L. Grisham, F.C. Jobes, D.W. Johnson, D.K. Mansfield, S.S. Medley, W. Morris, H.K. Park,

J.F. Schivell, G. Taylor, K.L. Wong, S. Yoshikawa, M.C. Zarnstorff and S.J. Zweben, J. Nucl. Mater. **145-147** (1987) 186.

[18] G.M. McCracken, J. Allen, K. Axon, R. Barnsley, S.J. Firlding, D.H. goodall, N. Hawkels, J. Hugill, P.C. Johnson, G.F. Matthews and C.S. Pitcher, J. Nucl. Mater. **145-147** (1987) 181.

[19] T.E. Stringer, in Proc. 12th European Conf. on Controlled Fusion and Plasma Physics, Budapest, Hungary, 1985, contributed papers, Part I, P. 86.

[20] P. Carolan and V. Piotrowicz, Plasma Phys. **25** (1983) 1065.

[21] T. Nishitani, K. Nagashima, T. Sugiyama, M. Hara, H. Takeuchi and JT-60 Team, Rev. Sci. Instrum. **59** (1988) 1866.

[22] T. Nishitani, K. Nagashima, T. Sugiyama, S. Koide and H. Takeuchi, Kakuyugo Kenkyu **59** Suppl. (1987) 243.

[23] H. Kubo, T. Sugie, A. Sakasai, Y. Koide, N. Nishino, H. Yokomizo, H. Takeuchi, JT-60 Team, K. Tanaka, H. Maezawa and N. Yamaguchi, Rev. Sci. Instrum. **59** (1988) 1515.

[24] T. Fukuda and A. Nagashima, Rev. Sci. Instrum. **60** (1989) 1080

[25] B. Lipschultz, J. Nucl. Mater. **145-147** (1987) 15.

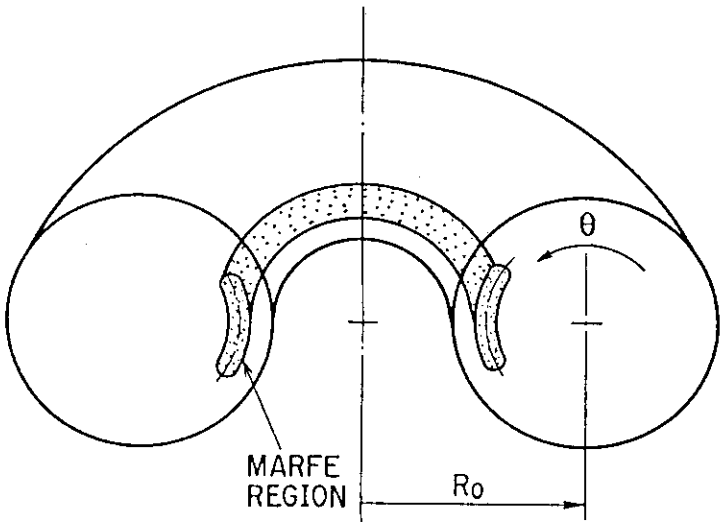


Fig. 1 Illustration of the marfe. The poloidal angle, θ, is measured from the outside midplane.

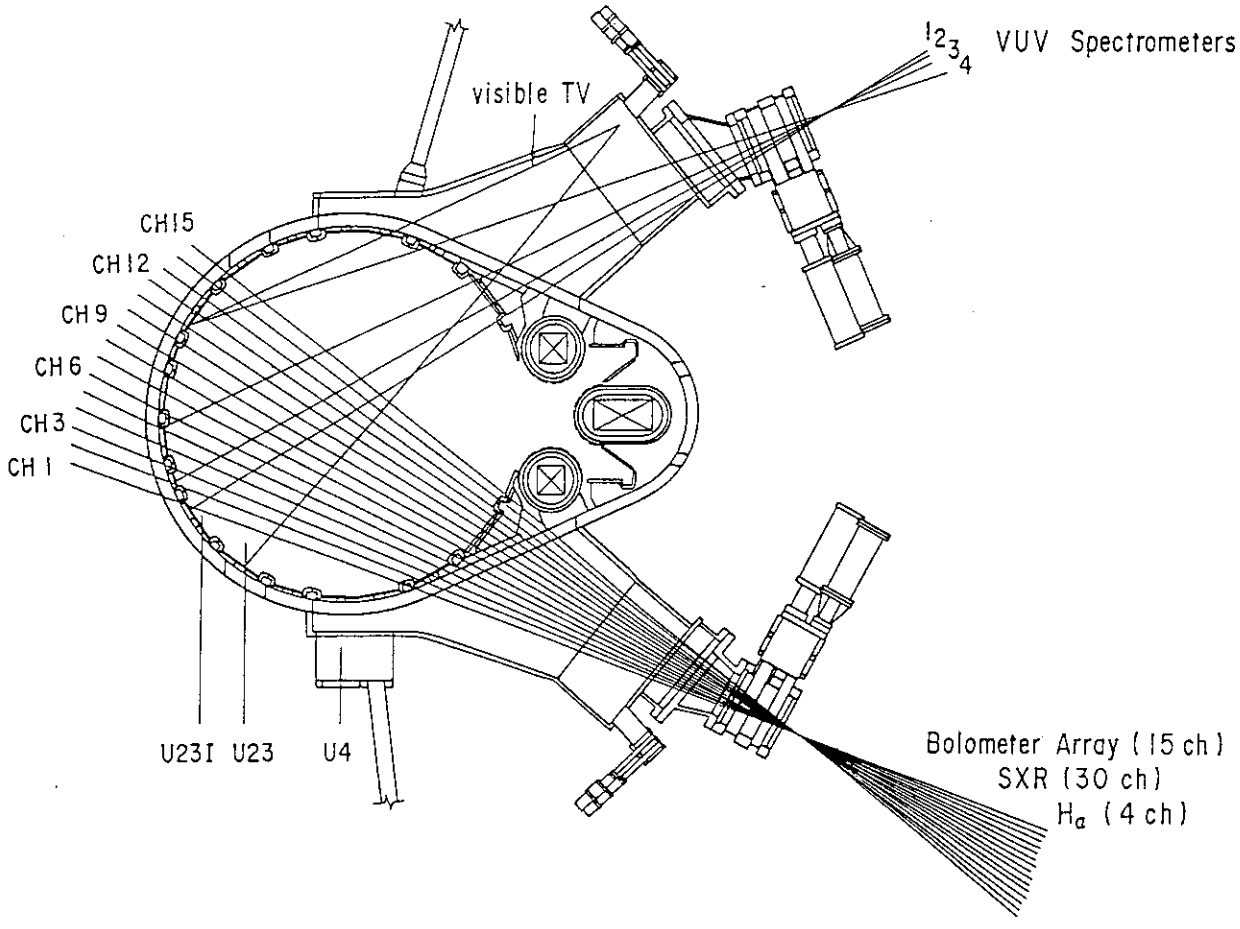


Fig. 2 Sightlines of the diagnostics concerned with the marfe observation on JT-60

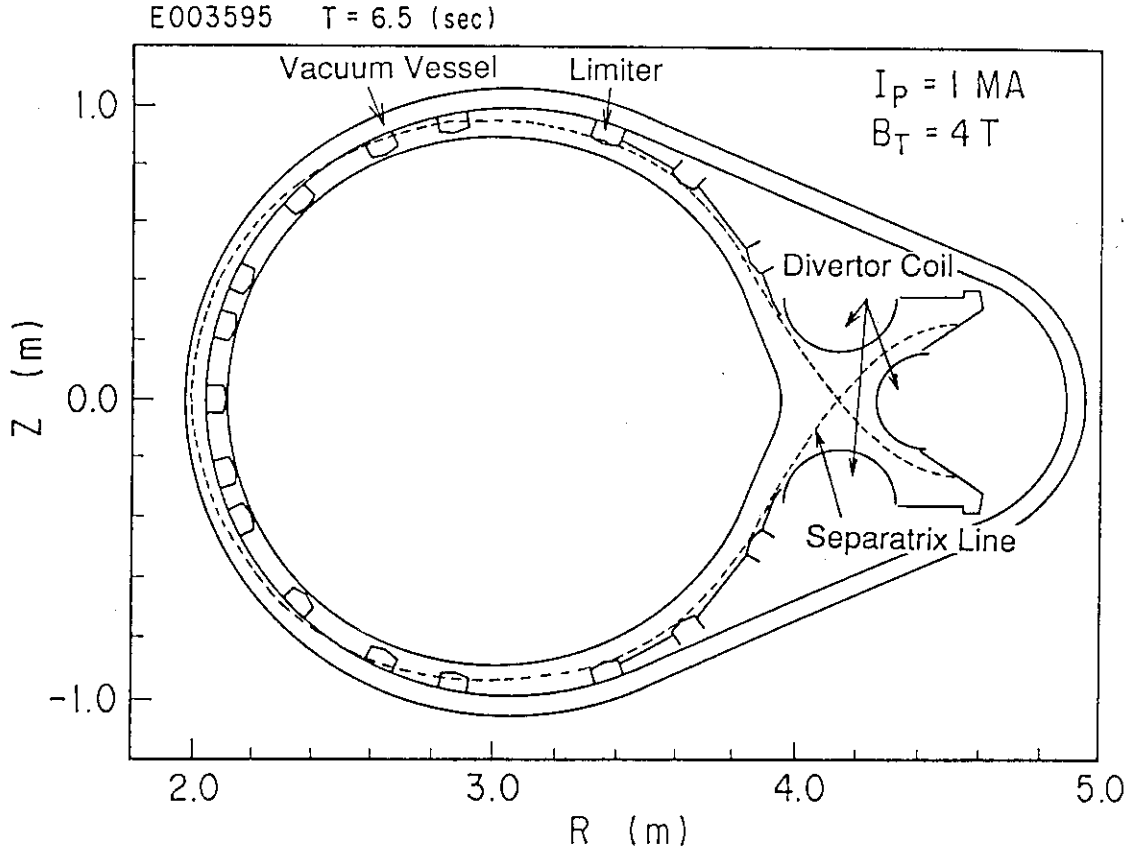


Fig. 3 Magnetic configuration of the ohmic discharge with the marfe. The plasma had a separatrix line and touched to the inboard limiter by exciting the divertor coil weakly.

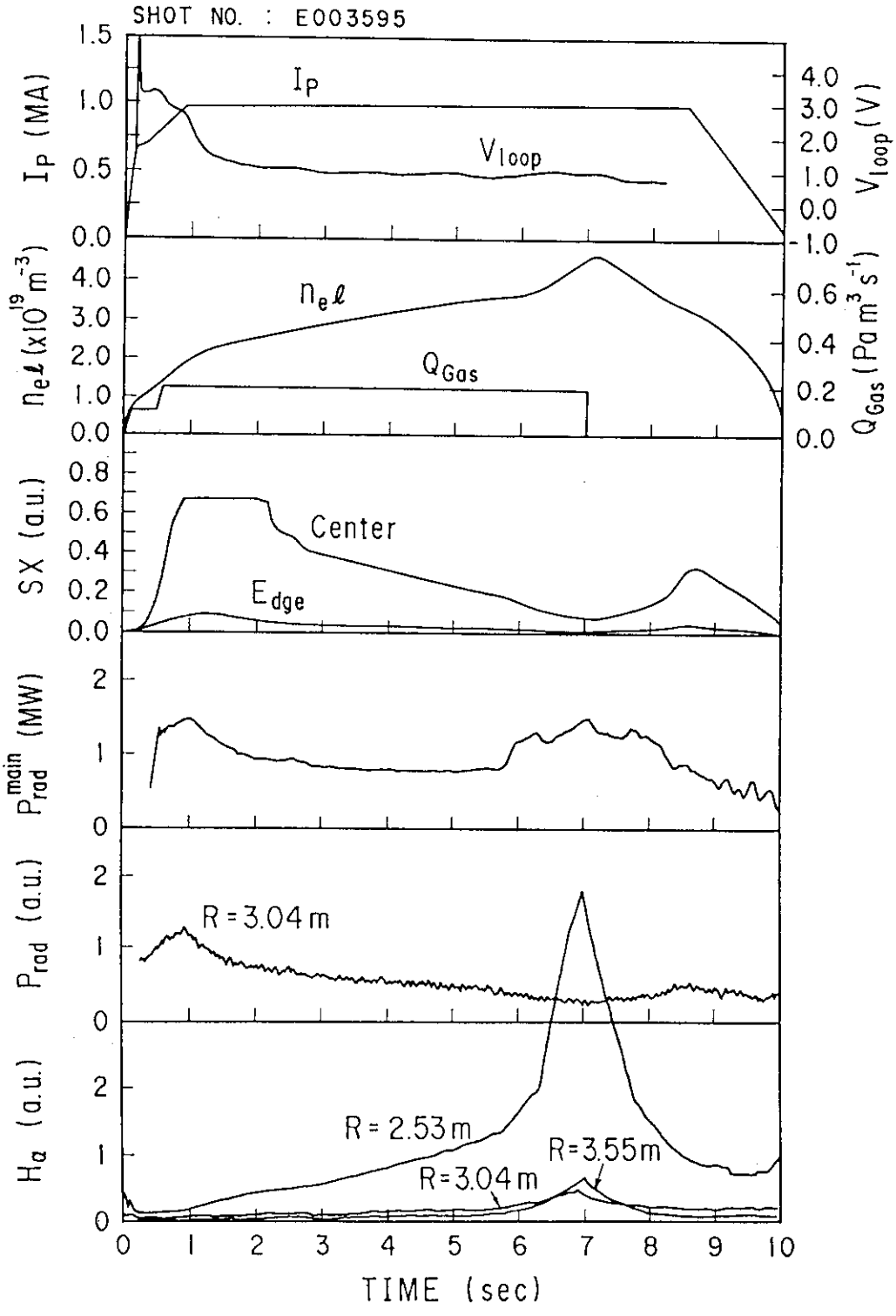


Fig. 4 Typical waveforms of the marfe in ohmically heated plasma

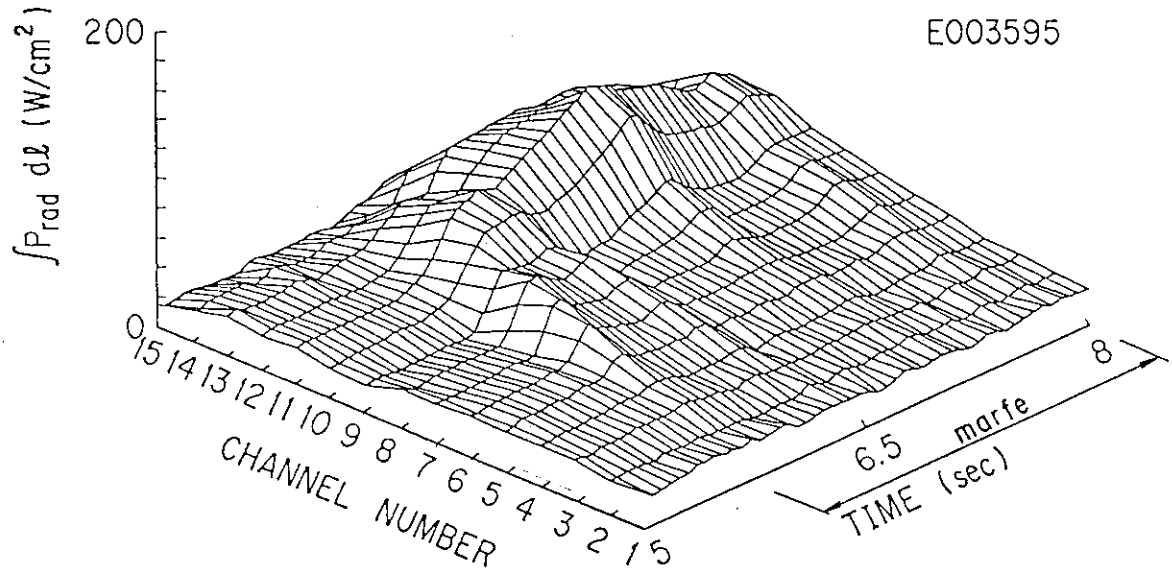


Fig. 5 Time evolution of the chord-integrated radiation losses in ohmically heated plasma with marfe.

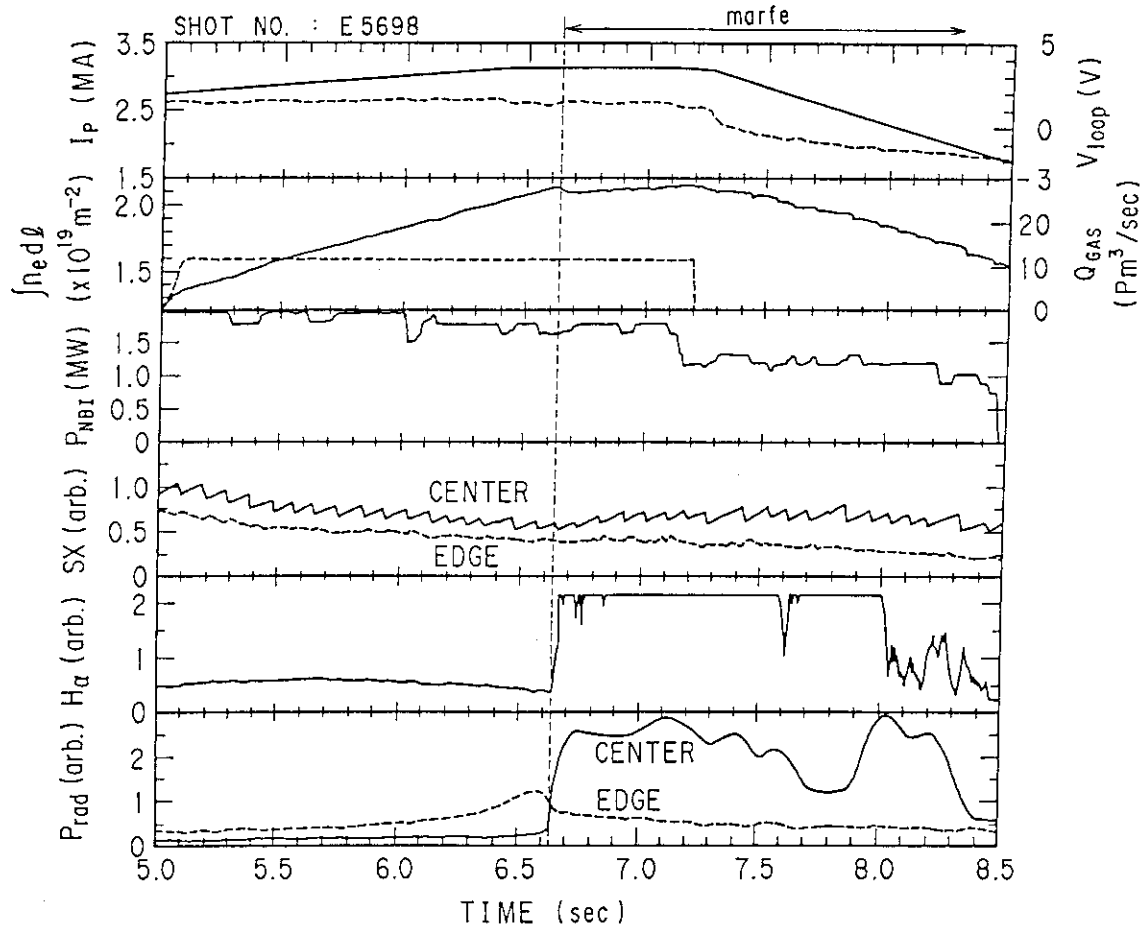


Fig. 6 Typical waveforms of the marfe in NB heated plasma

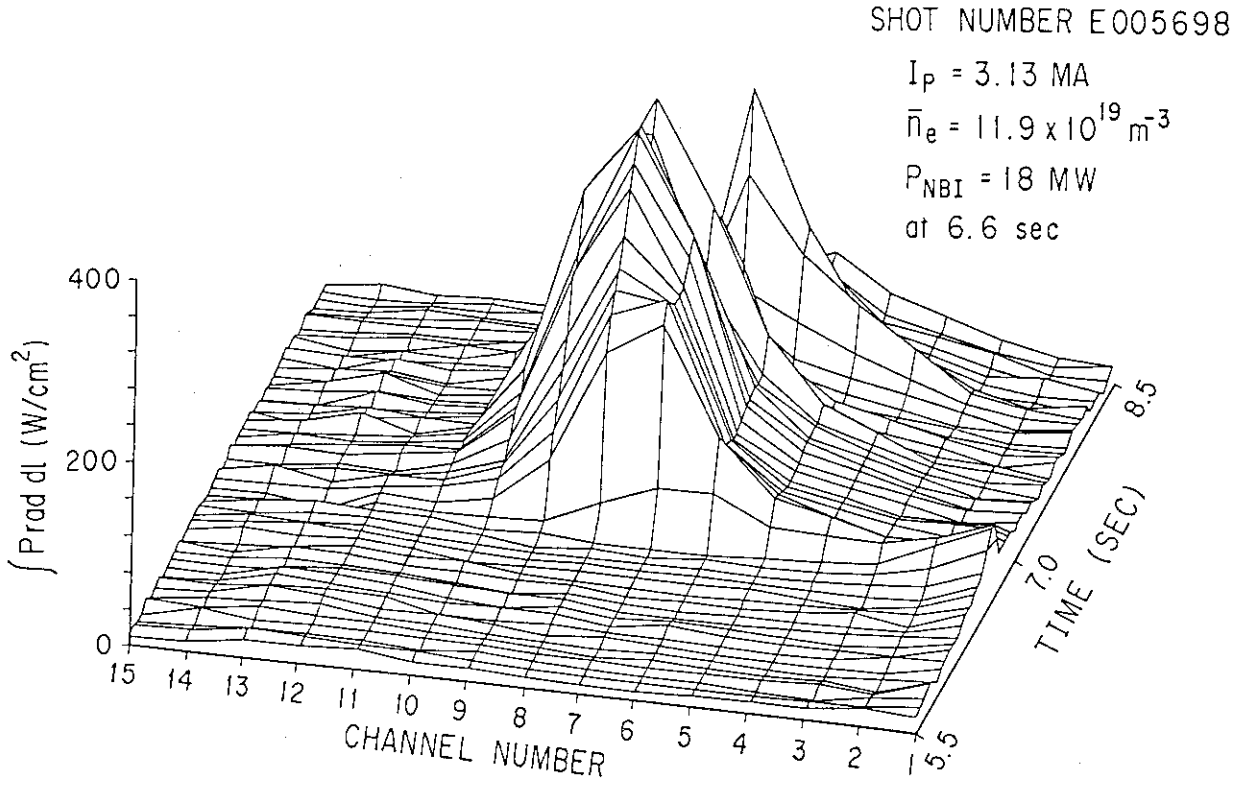


Fig. 7 Time evolution of the chord-integrated radiation losses in NB heated lasma with marfe.

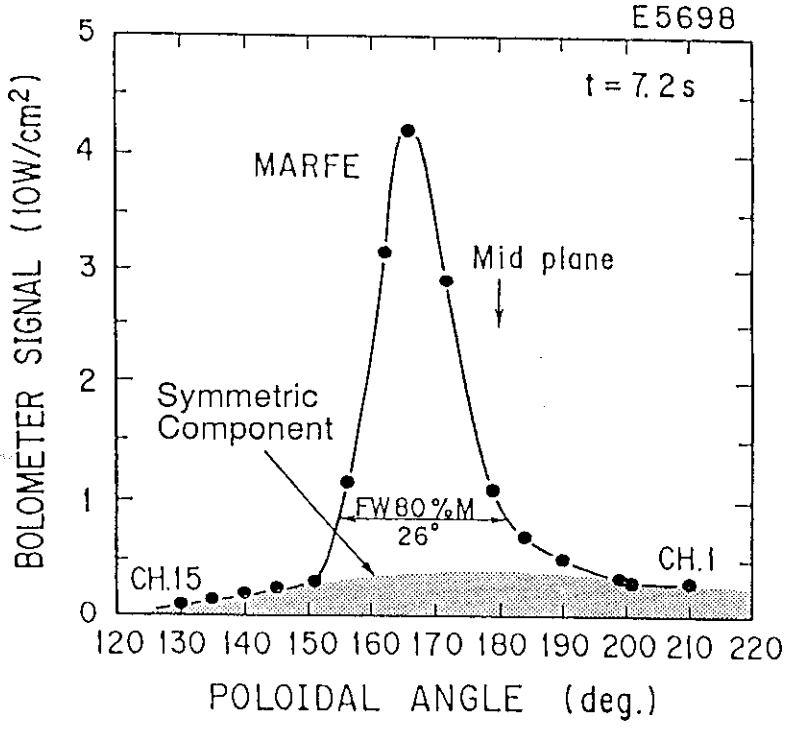


Fig.8 Poloidal extent of the marfe. The center of the marfe is about 10° above the midplane and the FWHM of the radiative band is 15° of poloidal angle.

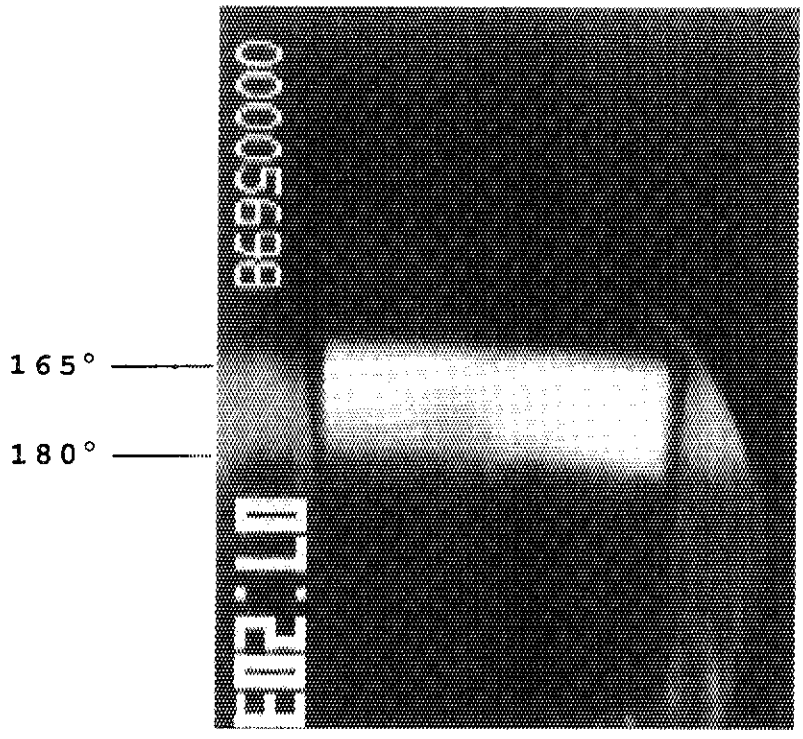


Fig. 9 Marfe observed by the visible TV camera. The bright emmision band is the marfe.

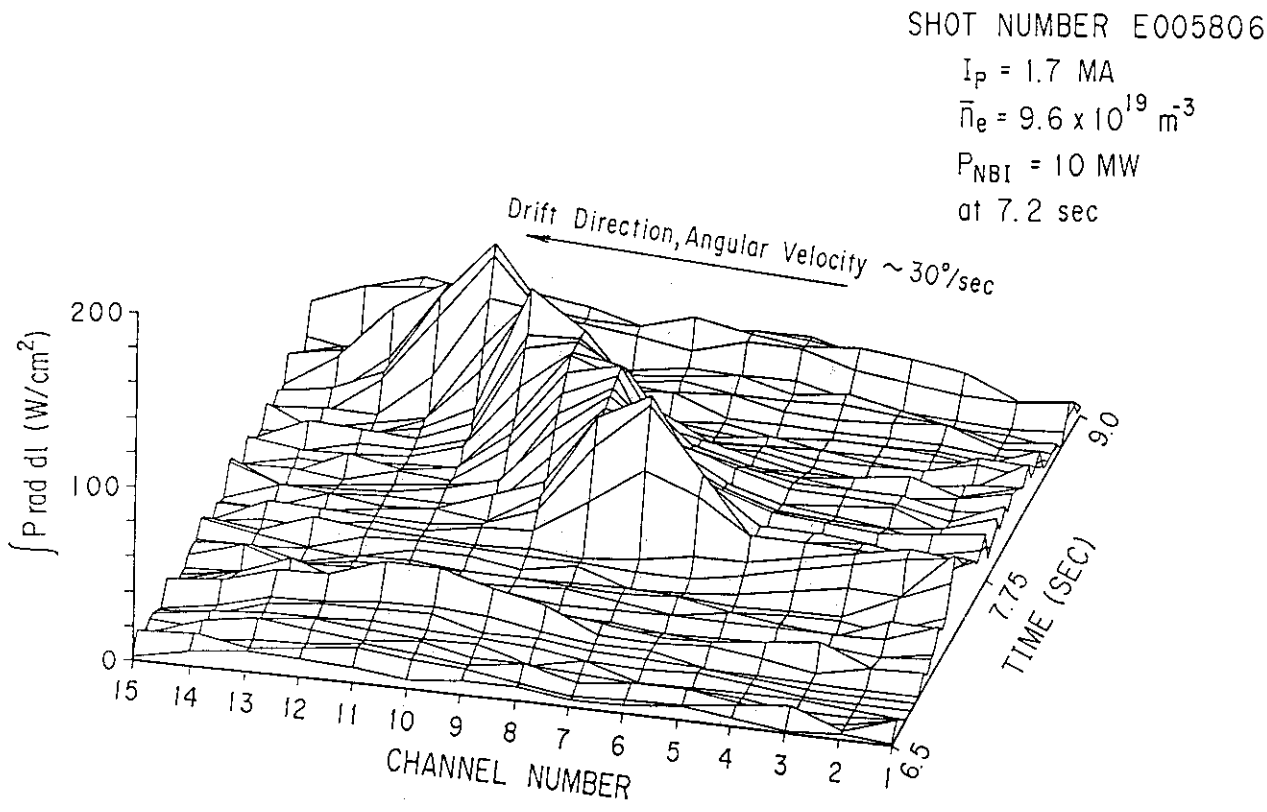


Fig. 10 Time evolution of the chord-integrated radiation losses showing drifting marfe.

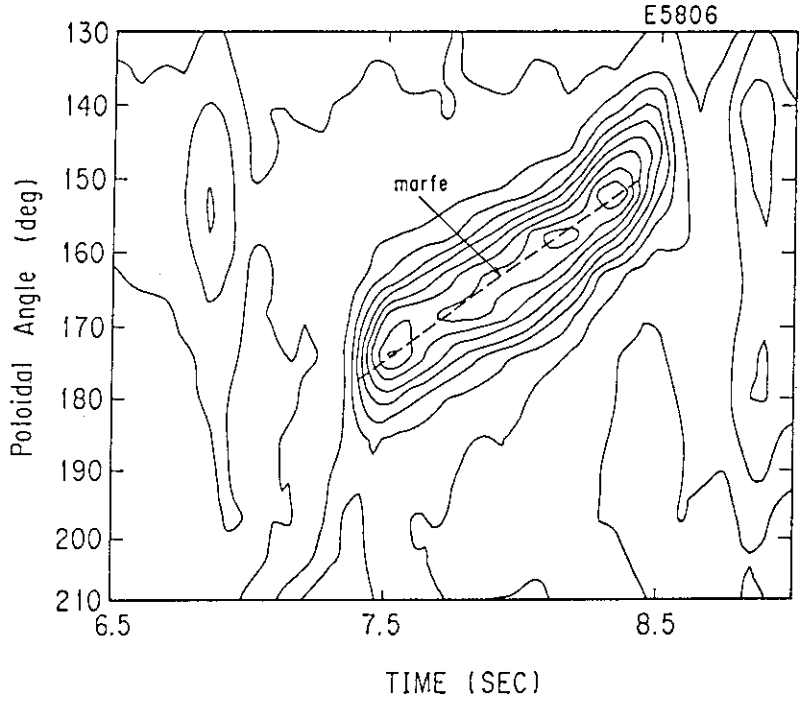


Fig. 11 Contour plot of time evolution of the chord-integrated radiation losses showing drifting marfe.

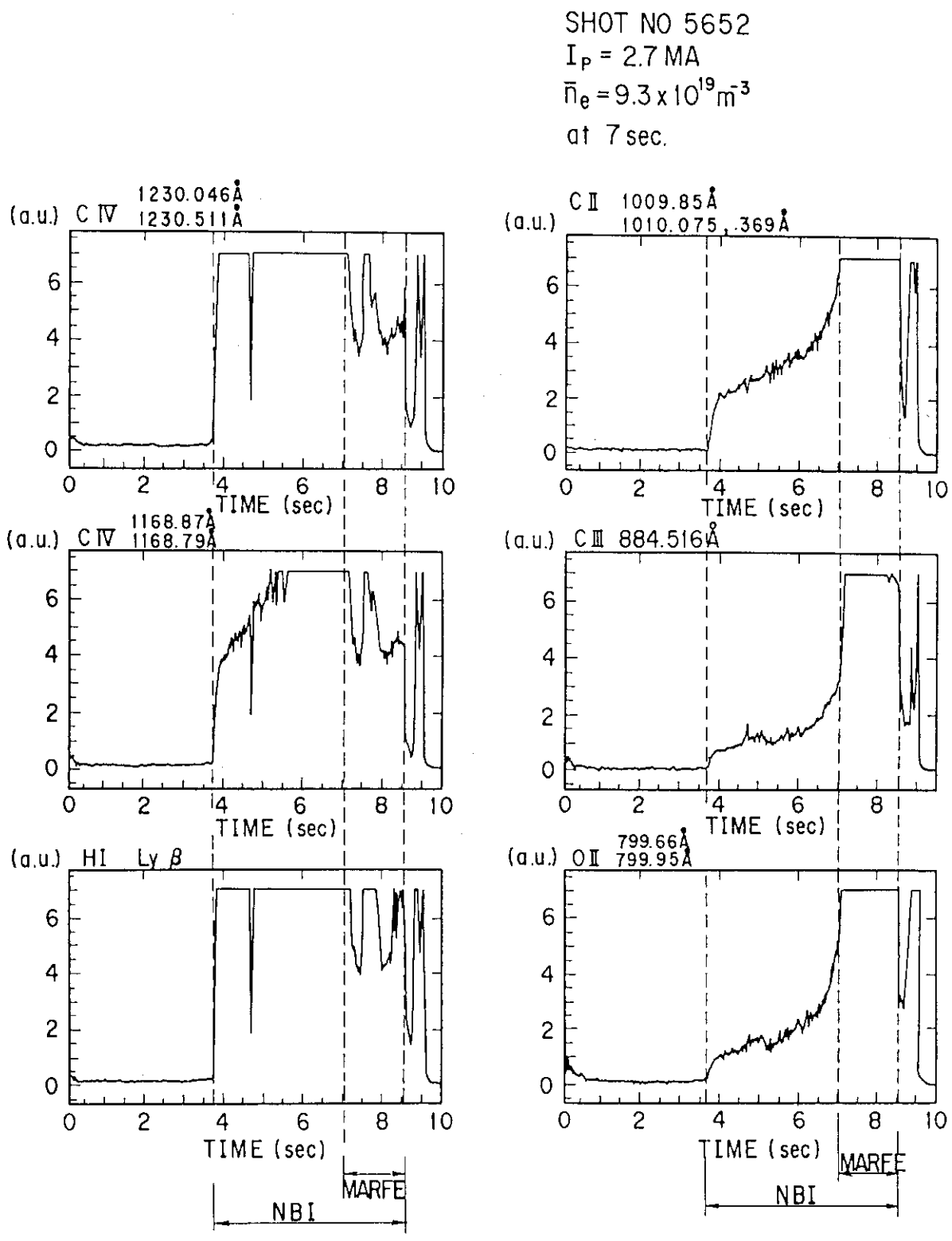


Fig. 12 Time evolutions of light impurity brightness in the marfe measured by the normal incidence spectrometer

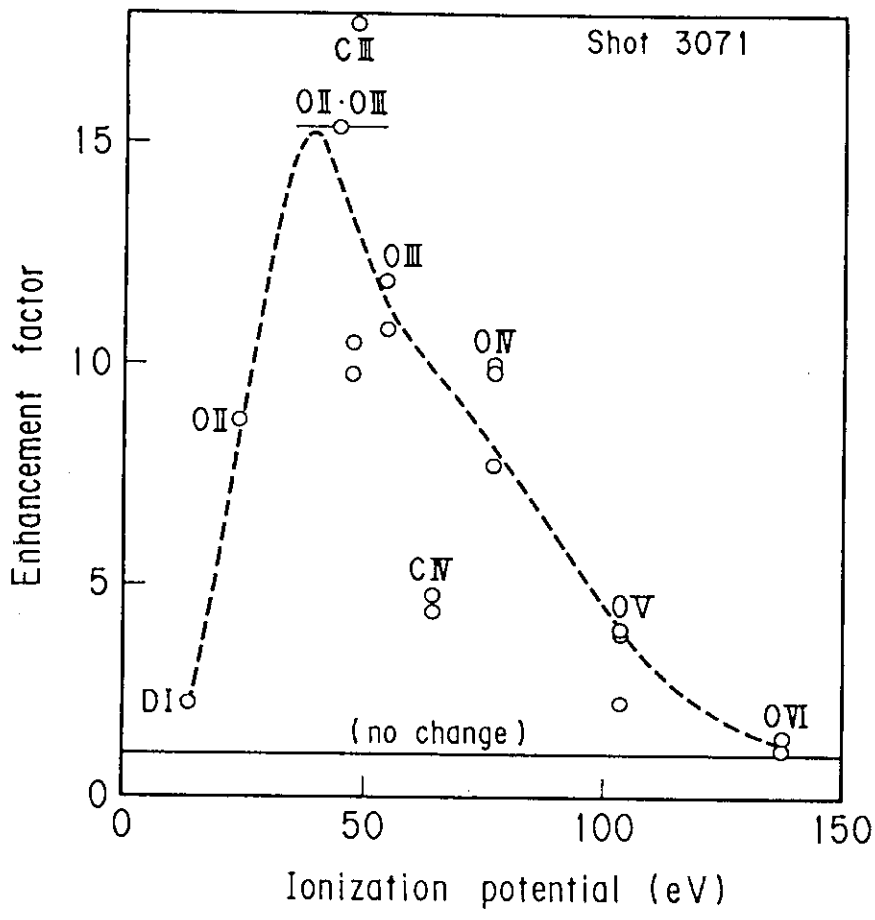


Fig. 13 Enhancement factors of low-ionized carbon and oxygen by marfe onset investigated quantitatively in JET

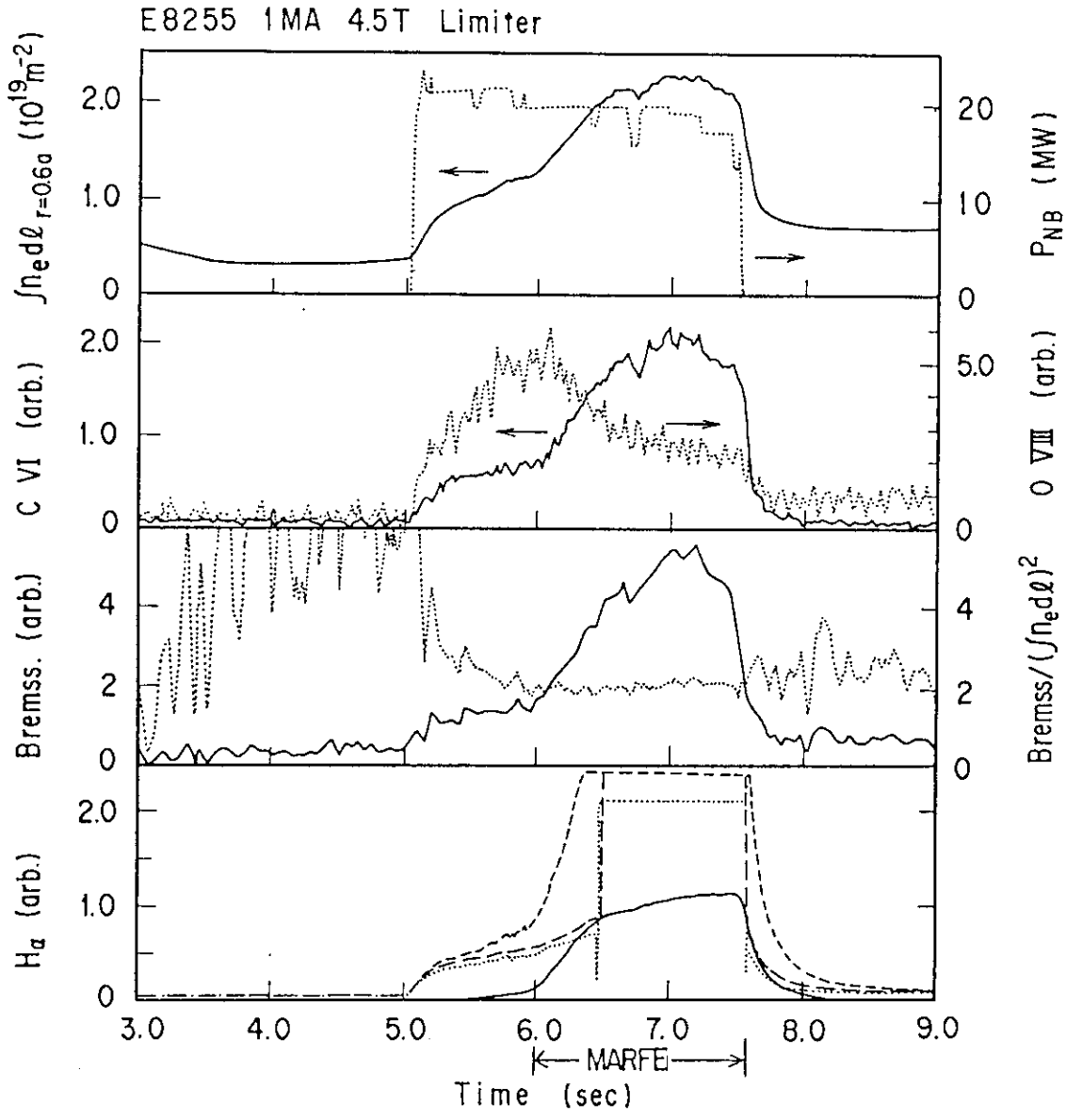


Fig. 14 Diagnostics wave forms of the marfe in relatively low density and plasma current plasma with NB heating

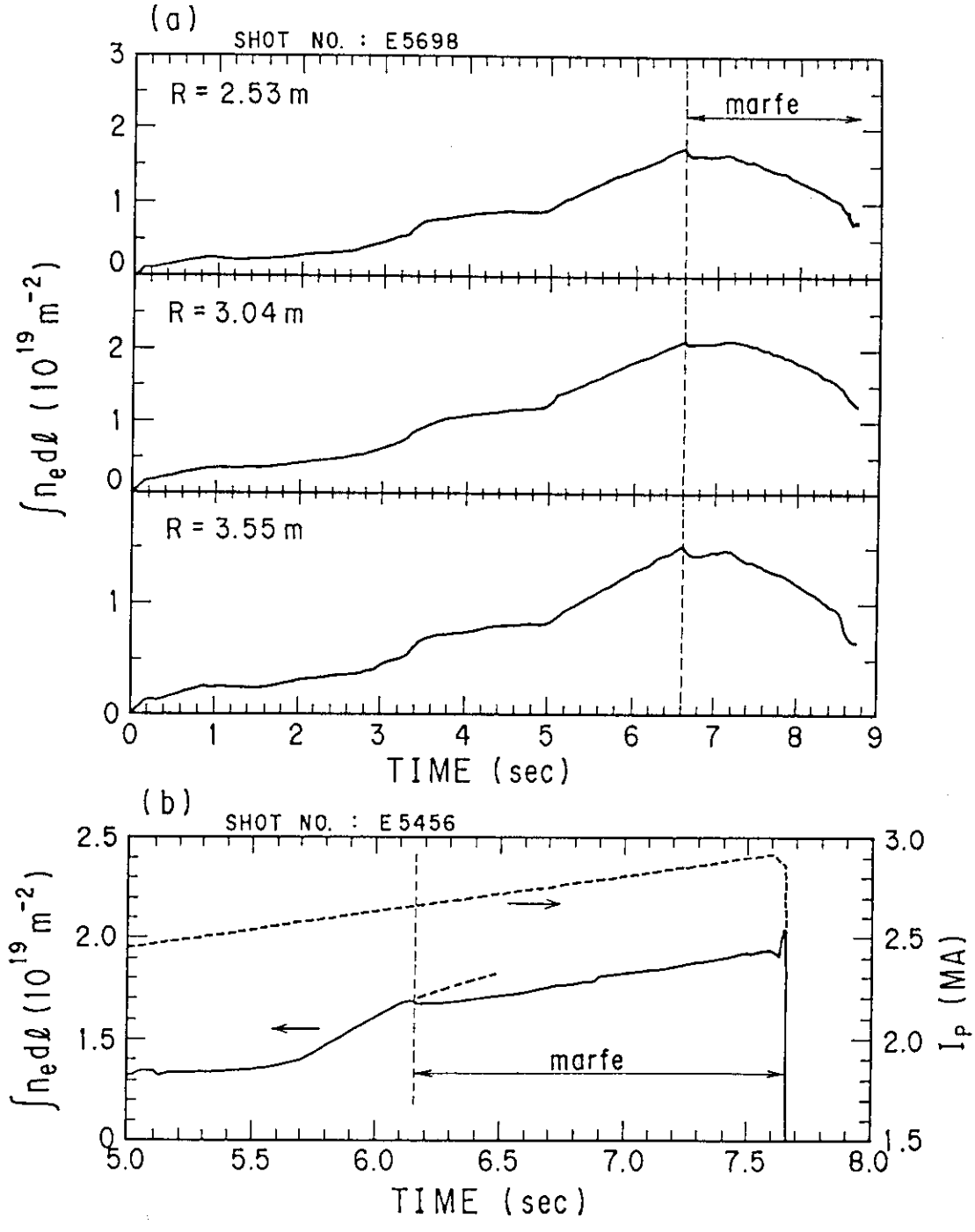


Fig. 15 Density behaviors in the marfe. (a) The increases of chord-integrated electron densities along the three vertical chords at R=2.53, 3.04 and 3.55 m are saturated with same manner at the marfe onset in spite of continuous gas puffing. (b) the chord-integrated density decreases ones at the marfe onset and keeps rising within the marfe period resulting in a major disruption at density limit.

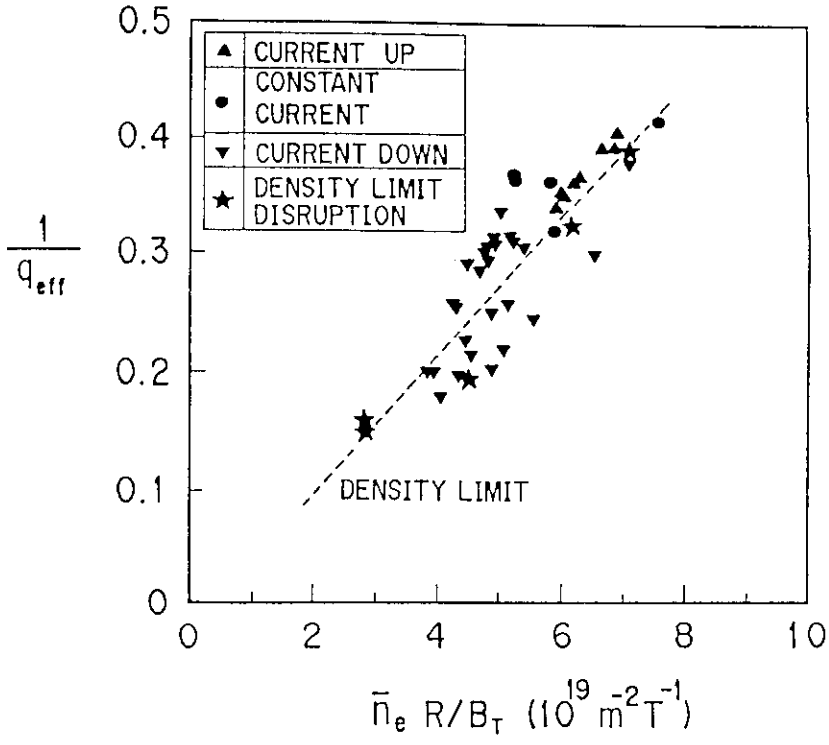


Fig. 16 Hugill diagram of the plasma at the marfe onset and the plasma disrupted by density limit.

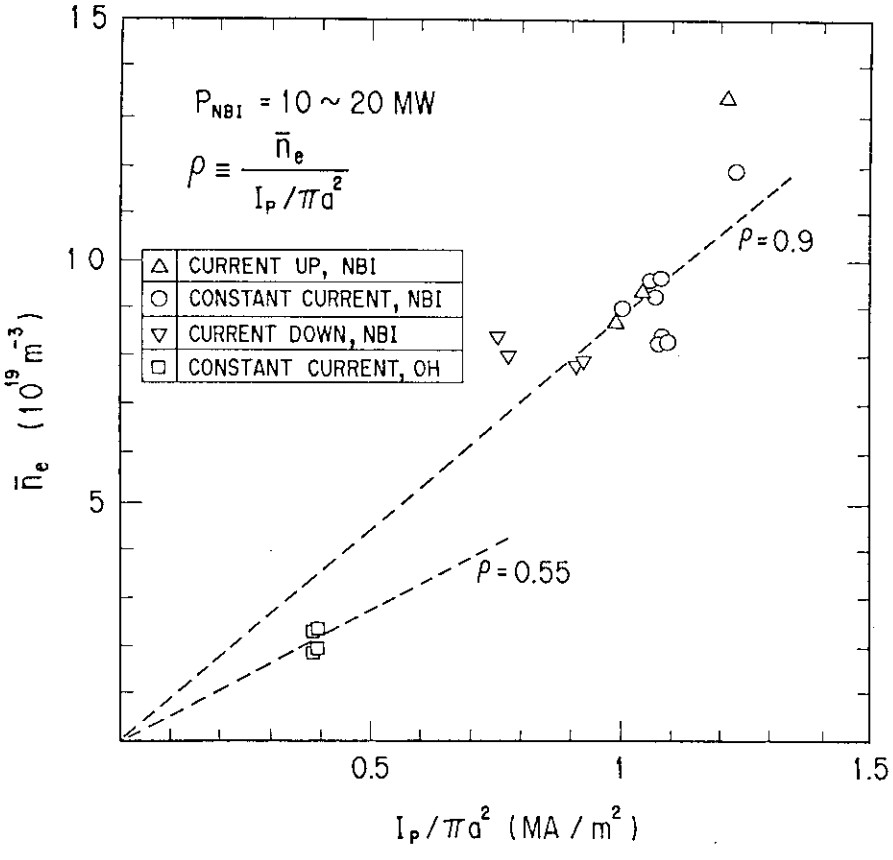


Fig. 18 Threshold electron density for the marfe onset plotted against the plasma current normalized by the poloidal cross-section of the plasma.

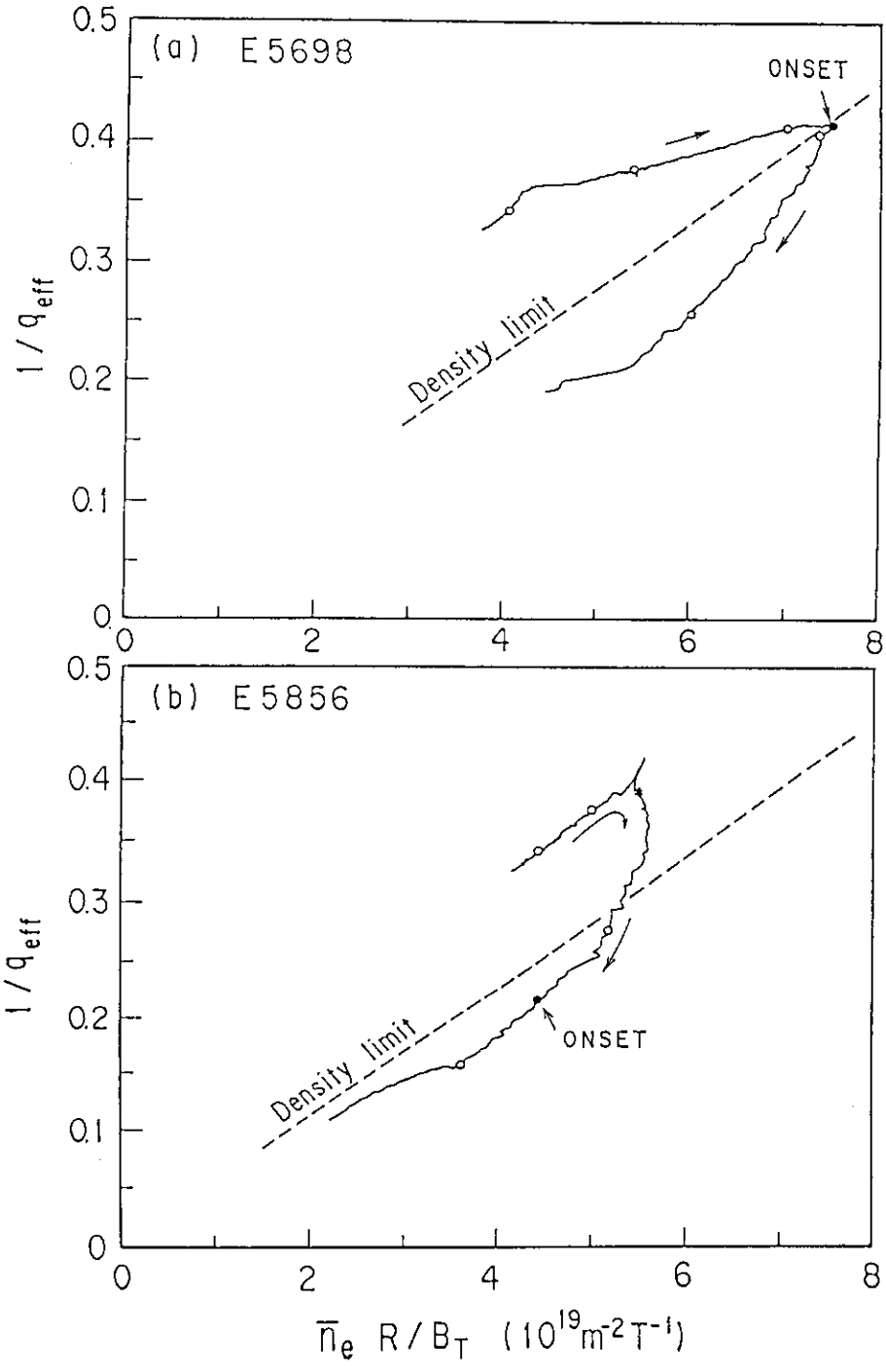


Fig. 17 Time trajectories of the plasmas with marfe onset at (a) constant $I_P$ phase and (b) decreasing $I_P$ phase.

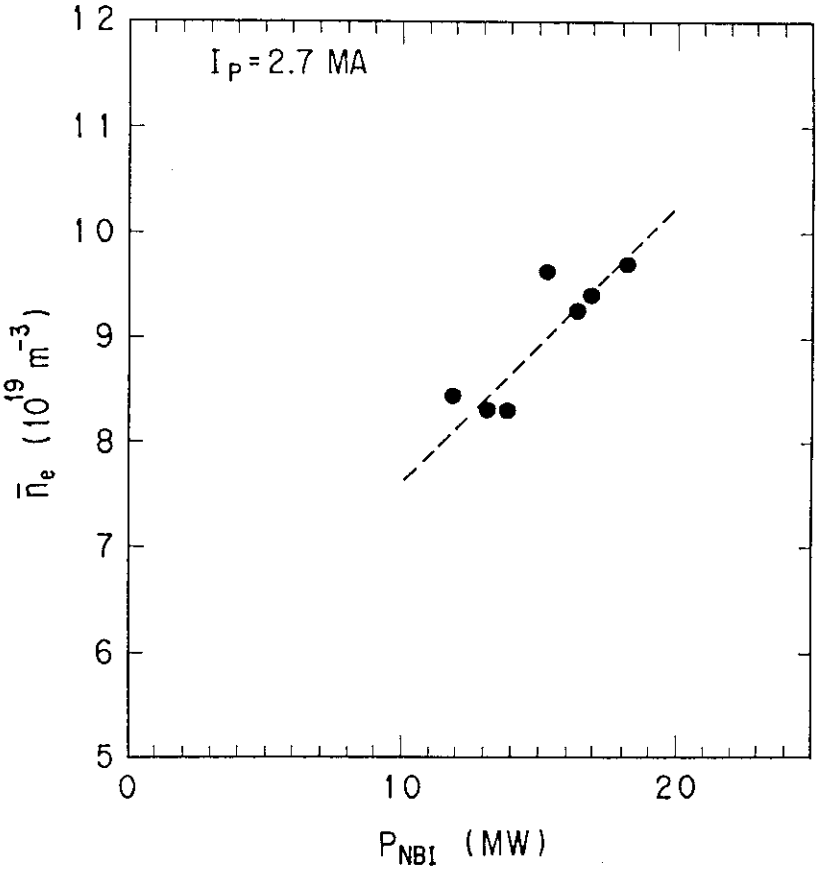


Fig. 19 Threshold electron density for the marfe onset plotted against the NB power in the discharges with $I_P$ = 2.7MA.

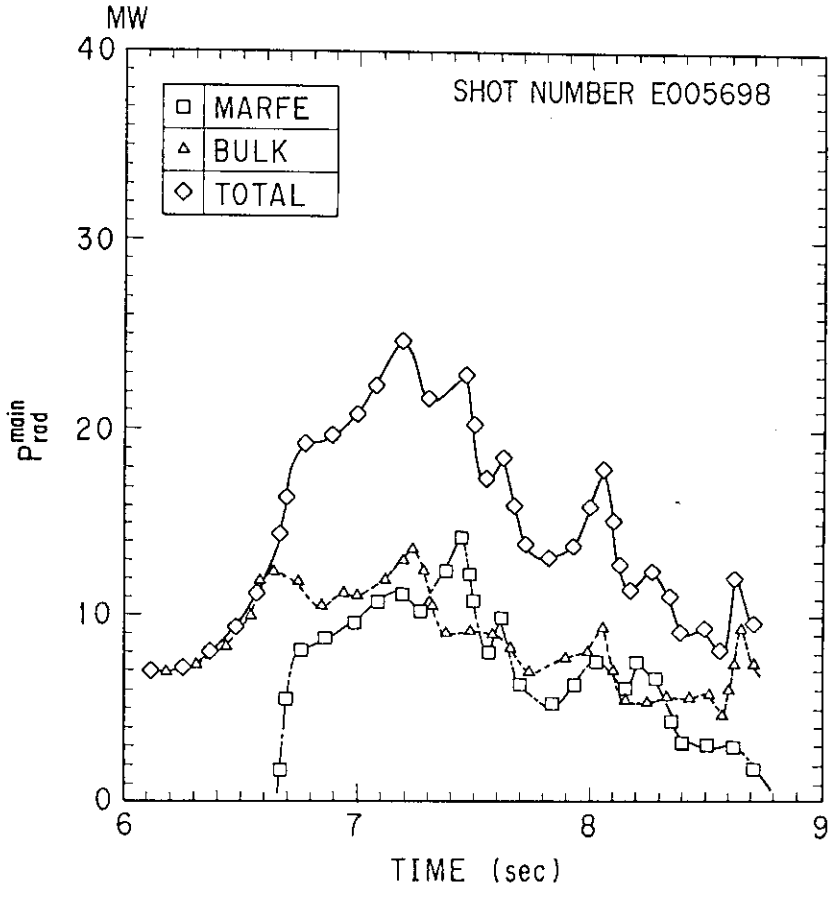


Fig. 20 Time evolutions of the symmetric and marfe components of the total radiated power for the plasma as for Fig. 4.

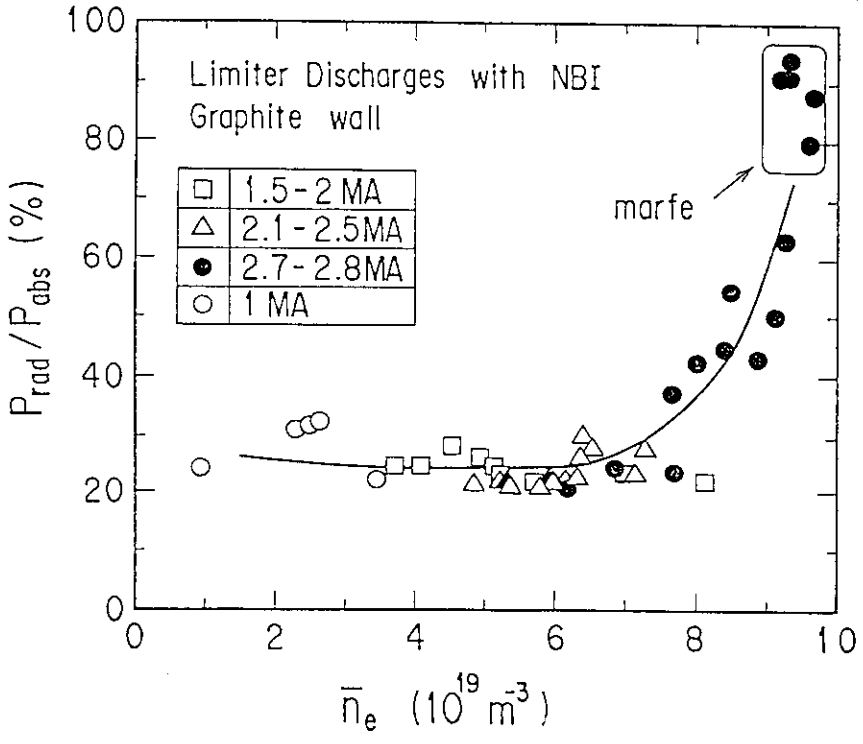


Fig. 21 Fractional radiated power to the absorbed power in the NB heated limiter discharges with graphite first wall as a function of $\bar{n}_e$.

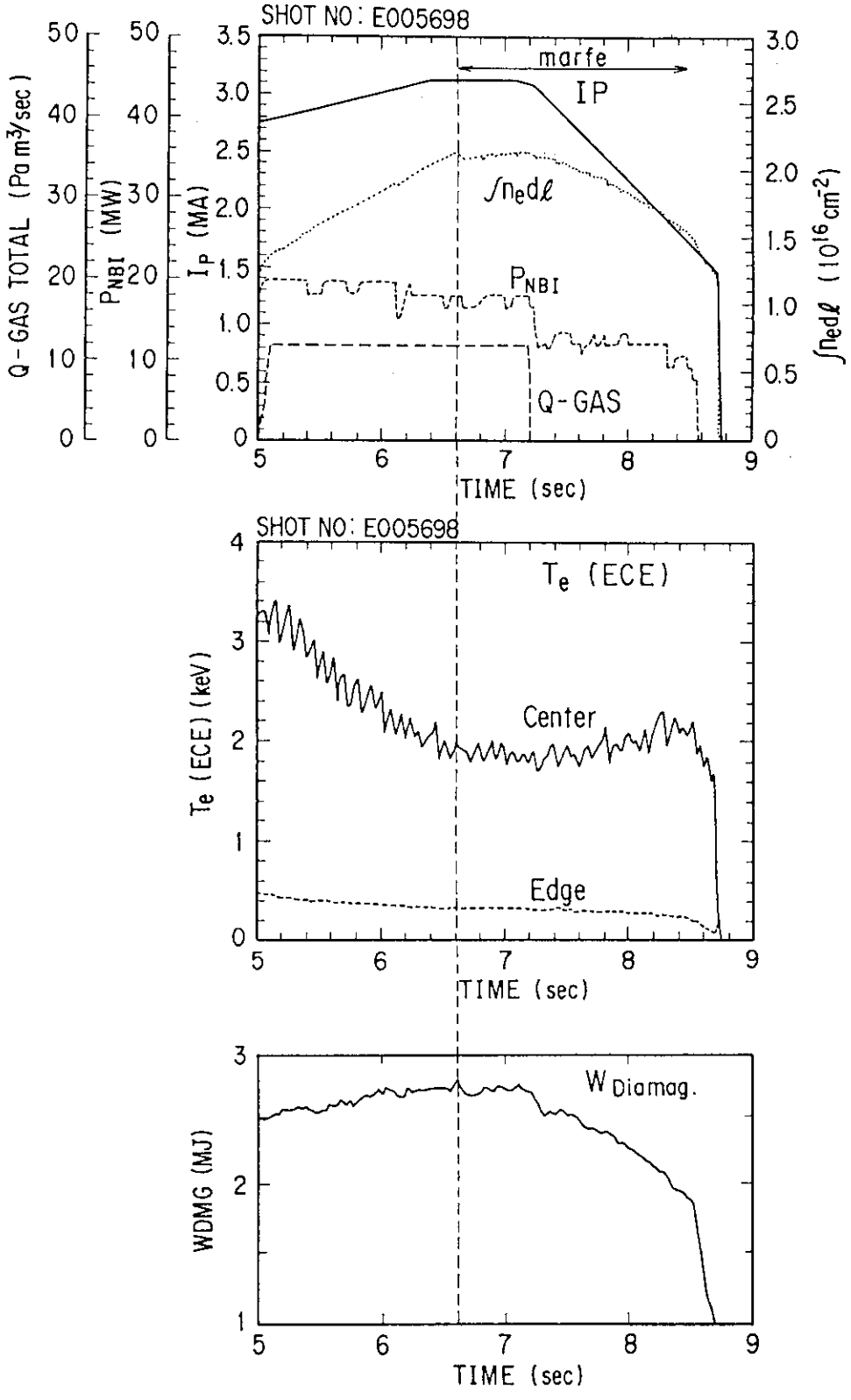


Fig. 22 Time evolutions of the stored energy measured by the diamagnetic loop, the electron temperature measured from the ECE emission, and other parameters as for Fig. 4.

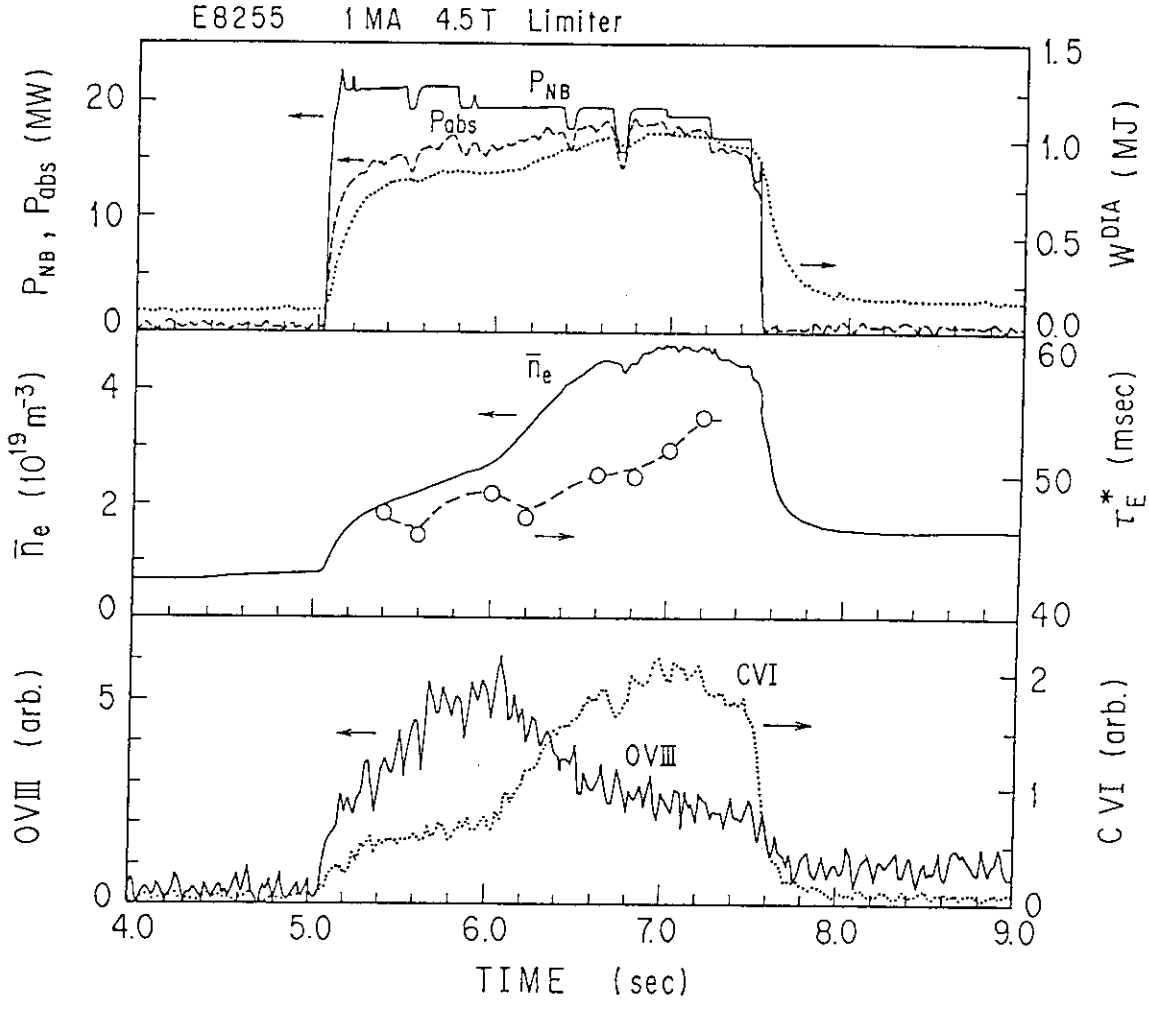


Fig. 23 Time evolutions of the stored energy measured by the diamagnetic loop, the energy confinement time and other parameters as for Fig. 11.